THOR 50M SUITABILITY FOR AUTOMATED VEHICLE CRASHWORTHINESS

Z. Jerry Wang, Jianying Li, Kartik Pallavajhala, Zaifei Zhou
Humanetics Innovative Solutions, Inc.
USA

Jingwen Hu, Kyle Boyle, Mathew Reed
University of Michigan Transportation Research Institute
USA

Paper Number 19-0162

ABSTRACT

The objective of this study is to use finite element (FE) models to understand the differences in response between human body model (HBM) and THOR-50M dummy in reclined seating scenarios that may become more common in automated vehicles. The **T**otal **Hu**man **M**odel for **S**afety (THUMS) v4.01 and Humanetics THOR-50M Anthropomorphic Test Device (ATD) FE model were used in both frontal- and rear-impact scenarios. The seating postures were based on data from a recent volunteer study. Front and rear impacts with seatback angles of 23, 33, and 43 degrees were simulated for a total of six test conditions. A US NCAP midsize sedan pulse was selected for the analysis. A publicly available seat model based on a 2012 Toyota Camry driver seat and a model of a ZF seatbelt system with pre-tensioner and load limiter were used in the study.

Both dynamic and kinematic data were analyzed and compared between the THUMS and THOR models, including motion, load measurements and displacements at numerous anatomical positons and sensor measurement locations. In addition, the seat cushion and seatback contact forces were compared. Due to the anthropometry discrepancies between the two models, the sensor measurement locations in THOR 50M do not necessarily coincide with THUMS anatomical locations. In such case, the anatomical location in THUMS was selected. The responses between the two FE models were similar in some parameters and quite different in others. The study could not determine which FE model has better biofidelity because no biofidelity specifications from Post Mortem Human Subject (PMHS) testing are available for such assessment.

INTRODUCTION

Future Automated Vehicles (AV) may offer new opportunities to restructure vehicle seat configurations to promote riding comfort or interactions among occupants [1]. AV show cars have proposed seat configuration that can be changed to facilitate better interactions between occupants, such as rear-facing in front row, diagonal cross seating, or other orientations. A widely anticipated scenario involves seatback angles that are more reclined for riding comfort or resting. However, these seat configurations pose challenges for the occupant protection. Kitagawa et al [2] studied the influence of seating position, direction and seating orientation on occupant responses with THUMS for autonomous vehicles. The study presented the challenges in various crash scenarios, including the interactions among the occupants in non-traditional seating configurations.

This paper focuses on the existing vehicle fleet with an extended scope, i.e. rearward facing seating. Oblique and side impact scenarios are not covered in this paper. Since there is a lack of PMHS data available for these crash scenarios, finite element model simulations were used to understand the difference between the HBM and the ATD FE models. To the authors' knowledge, none of the FE models have been validated in these seating configurations in crash testing. This analysis focuses on the upper-body kinematics and output from the ATD sensors and the corresponding outputs from THUMS. Lower extremities were not analyzed since there was no vehicle interior representation that would interact with the lower extremities in the study.

METHODS

Analysis Tools

LS-DYNATM Version 971 (Livermore Software Technology Corporation, USA), a general –purposed FE simulation package was used for the analysis. Toyota Camry 2012 driver seat FE model was used for the simulation [3]. ZF seatbelt model with retractor pre-tensioner and load limiter was from a previous project of University of Michigan Transportation Research Institute (UMTRI). THUMS version 4.01 [4] [5] was selected as the HBM and Humanetics THOR-50M FE model v1.6 was used for the comparison analysis.

Occupant Positioning Guidelines

Before the simulation work, a project at UMTRI studied the volunteer seating postures in reclined seatback configurations [6]. The study measured critical landmarks in different seatback angles. A regression model was generated from the human volunteer measurements to represent the occupant seating postures, including head orientation, spine position, pelvic bone orientation and lower leg positions.

THUMS Sensors

Load cell representations were created in THUMS at the corresponding locations in the THOR-50M model. Linear accelerations and angular rate were extracted from THUMS at the corresponding sensor locations in THOR-50M as well. Pre-simulation was used to position the THUMS 4.01 model according to the seating posture defined in [6]. The THUMS head orientation, T1, T4, T8, T12, pelvis orientation, hip joint, knee joints, and ankle joints are prescribed to match the occupant seating postures obtained from UMTRI[6].

ATD Positioning

The ATD was studied in CAD to best match the seating posture defined in [6]. The hip joint was aligned first, then the ATD dummy pelvis was rotated until pelvic bone matched the occupant seating orientation. Next, the lower spine joint was adjusted to match the target spine position, and the upper spine joint was adjusted to match the target head orientation. The thighs were adjusted to match the orientation between the hip and the knee joint center, and finally the lower leg was adjusted accordingly. The ATD thoracic joint setups are summarized in Table 1. The ATD seating postures in various seatback angle are shown in Figure 1. A round bar was placed in the front of the lower leg to prevent the legs from flailing.

Table 1.
THOR-50M thoracic joint pitch positon for each seatback angle

Seatback Angle	Pelvis Angle	Lower Spine Pitch Positon	Upper Spine Pitch Positon
23°	33°	-12° (yellow mark)	0°
33°	36.3°	-3°	0°
43°	39.6°	+6°	-3° (head forward)

a. 23° seatback angle b. 33° seatback angle c. 43° seatback angle

Figure 1. Side views of THOR-50M seating postures at 23°, 33° and 43° seatback angles

For 23° seatback angle positioning, NHTSA NCAP ATD positioning procedure was followed. The pelvis angle was set to 33°, then the lower spine joint was adjusted to best match the occupant spine position, see Figure 1a. It was

observed the head positon is quite off toward the rear direction comparing to Robbins 1983 [7] . This placed the THOR 50M head approximately 39 millimeters behind the UMTRI AMVO 50th male head location.

Crash Pulse

US NCAP mid-size sedan pulse was selected for the simulation, see Figure 2. The delta-V is 56km/hour and the peak acceleration is approximately 43 g. The pulse first returns to zero acceleration after 90 ms.

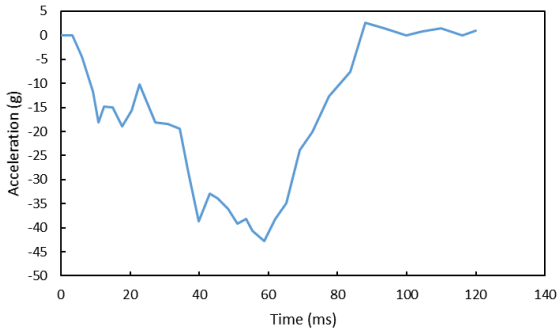

Figure 2. Sled pulse for both forward and rearward facing simulation.

RESULTS AND DISCUSSION

Forward Facing

Kinematics – Trajectory

The kinematics responses of the THUMS and THOR-50M FE models with 23°, 33°, and 43° seatback angles were compared at the head center of gravity location (CG), T1, T4, T12 and pelvis CG locations. The head rotation and the pelvis rotation were calculated from the angular rotational sensors and compared in this study. The THUMS model upper torso bends more than that of the THOR-50M model. The known stiff lumbar of THOR-50M may have contributed significantly to this difference. For the lower torso trajectories, it was noticed the THUMS model's forward motion is much higher than that of THOR-50M at all locations compared.

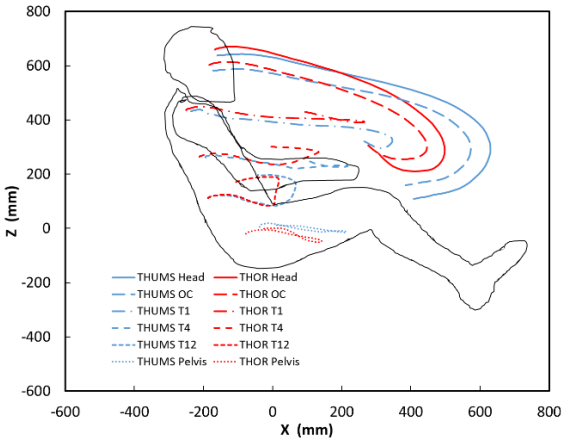

Figure 3. Trajectory comparison between THUMS and THOR-50M for 23° seatback angle, forward facing

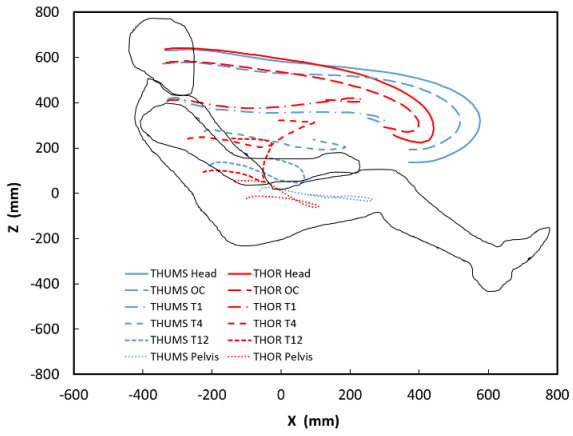

Figure 4. Trajectory comparison between THUMS and THOR-50M for 33° seatback angle, forward facing

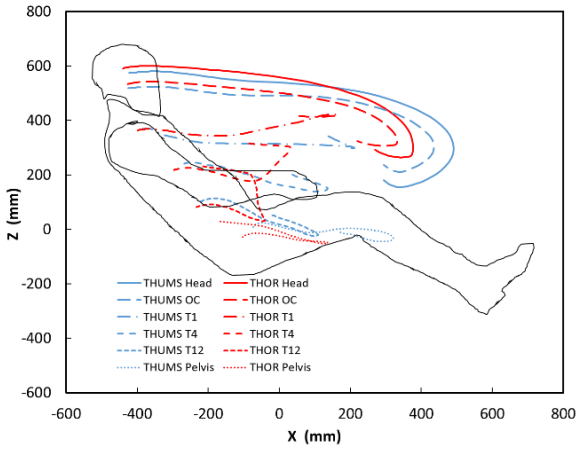

Figure 5 Trajectory comparison between THUMS and THOR-50M for 43° seatback angle, forward facing

Head

The head accelerations and head rotations are shown in Figure 9 through Figure 12 in Appendix I. The head resultant accelerations are very comparable in all three seating postures between THOR-50M and the THUMS models. The spikes near 0.13 second time mark were due to the head-knee contact during the impact, see Figure 9. In x-direction, THOR-50M head rotation started earlier than that of the THUMS model, and its maximum rotation is much lower, see Figure 10. In y-direction, the THOR-50M and THUMS rotations were similar. However, the THOR-50M rotation rose faster later in the event, and the maximum rotations were comparable, see Figure 11. In z-direction, the THUMS head rotation is much faster than THOR-50M, and the maximum rotation is much more than the THOR 50M in 23° and 33° seatback angles. Since THOR-50M dummy neck does not have a human-like low resistance in torsion up to approximately 40 degrees from the neutral forward direction, this could be the reason that the THOR-50M z rotation is less than that of the THUMS.

Thorax Displacement - Upper Left IR-TRACC

The upper left thorax Displacement was caused by the torso interaction with the shoulder belt. In x-direction, the displacement in THOR-50M is higher than THUMS except for the 43° seatback angle configuration, see Figure 13 in Appendix I. In y- direction, the THUMS has much higher displacement, see Figure 14. In z-direction, both THOR-50M and THUMS moved downward, however the displacement magnitude for THUMS is much higher, see Figure 15. The THUMS model results showed more sinusoidal pattern in y and z direction, which also shown in the resultant acceleration. Higher displacement was observed at 43° seatback angle for both THUMS and THOR-50M models, especially in x and y direction, see Figure 13 and Figure 14.

Thorax Displacement - Upper Right IR-TRACC

The upper right thorax displacements were very comparable between THOR and TUMPS in x and z directions during the loading stage, and very different in the unloading stage, shown in Figure 16 and Figure 18 in Appendix I. In y direction, the ribs in both THOR-50M and the THUMS moved toward the right at the beginning, then the THUMS rib moved toward the left while the THOR-50M was still moving toward the right, shown Figure 17.

Thorax Displacement - Lower Left IR-TRACC

The lower left thorax x displacement was significantly lower than THUMS, see Figure 19 in Appendix I. It was noticed that the x-displacement at the corresponding position of the lower left IR-TRACC had positive displacement, which was caused by the internal organ movement when compressed by the seatbelt. It also moved downward by approximate 40 mm (z displacement) for THUMS model, a much higher magnitude than the THOR-50M, shown in Figure 19.

Thorax Displacement - Lower Right IR-TRACC

The lower right thorax x displacement for THUMS was much higher and it moved forward due to the organ movement when compressed by the seatbelt, see Figure 22 in Appendix I. On the contrary, the THOR-50M x displacement was in a much lower magnitude. In y and z directions, the displacement between THUMS and THOR-50M matches closely in the loading stage, see Figure 23 and Figure 24. In the unloading stage, THUMS model has much higher z displacement during the unloading stage, see Figure 24. The THUMS model y displacement was more sensitive to the seatback angle change, especially in the unloading stage, see Figure 23.

Abdomen Displacement

The left abdomen x displacement was similar between THUMS and THOR-50M, see Figure 25 in Appendix I. The x displacements of the THUMS was insensitive to the seatback angle change while the THOR-50M was quite sensitive in contrary. The lateral and vertical displacements were different between the two models, see Figure 26 and Figure 27. However, this is insignificant because of the relatively low magnitude. Similar responses were observed for the right abdomen displacements, see Figure 28 through Figure 30.

Pelvis Rotation and Acceleration

The pelvis y rotation was similar for 23°and 33° seatback angle within the two models. However, the y rotation for 43° seatback angle was in opposite direction for THUMS, see Figure 32 in Appendix I, which was most likely caused by the pelvis bone geometry difference and the lumbar stiffness, which could significantly affect the interaction with seatbelt. The THUMS pelvic bone is narrower than the THOR-50M, the relatively stiff THOR-50M lumbar provided a stronger coupling between the upper torso and pelvis, and therefore influenced the kinematics of the pelvis.

The oscillations of the pelvis acceleration for THUMS was prominent, shown in Figure 34 through Figure 37 in Appendix I. For 23° and 33° seatback angle, the pattern between the two models were comparable when ignoring the oscillations. The pelvis acceleration in x and z directions for 43° seatback angle differed from the other two seatback angles studied. The difference could be caused by the severe submarining behavior in both THOR and THUMS models.

Anterior Superior Iliac Spine (ASIS) Load

It was observed that the THUMS model tends to submarine more than THOR-50M for all three cases, evidenced by the animation and the low ASIS force and moments in both left and right sides, see Figure 38 through Figure 41. THOR-50M model did not submarine in 23° and 33° seatback angles, but submarined in 43° seatback angle.

Belt Force and Seat Pan Force

The belt tractor payout of the THUMS is slightly higher than that of THOR-50M, shown in Figure 42 in Appendix I, implying that the upper torso has more forward motion in THUMS. The shoulder force between the two models were comparable, see Figure 43. The lap belt force and occupant seat pan contact force for THUMPS are slight lower than these of THOR-50M, shown in Figure 44 and Figure 45.

Rearward Facing

In rearward facing cases, the seatback contributed significantly to restraint the occupant. It was found the Toyota Camry 2012 seat yielded during the rearward facing simulation without any reinforcement, which is not of the interest of this study. To address the problem temporarily, the seatback frame was rigidized. The occupant motion was in a much lower scale compared to the frontal impact when the seatback did not yield. The neck motion was largely influenced by the head restraint. There was no effort in this paper to explore the head restraint design options. However, the head restraint was positioned against the back of the head for each analysis.

Trajectories

It was noticed both THUMS and THOR-50M torso moved upward along the seatback, see Figure 6 through Figure 8. The neck ramped up and interacted strongly with the head restraint. The head restraint design is critical for the head and neck protection.

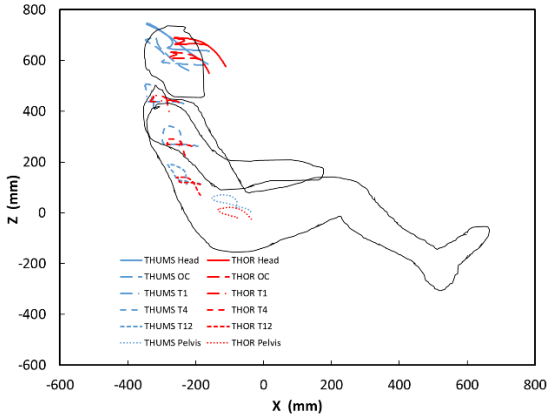

Figure 6. Trajectory comparison of THUMS and THOR-50M in 23° seatback angle, rearward facing

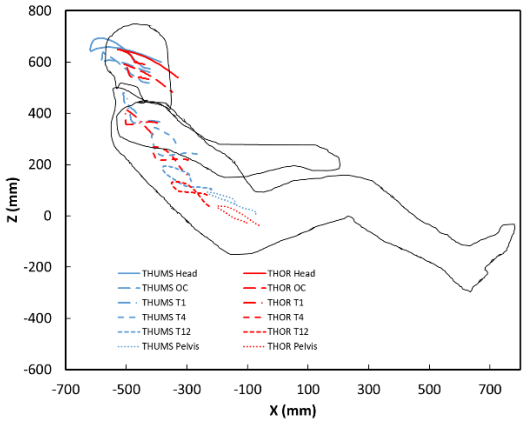

Figure 8. Trajectory comparison of THUMS and THOR-50M in 43° seatback angle, rearward facing

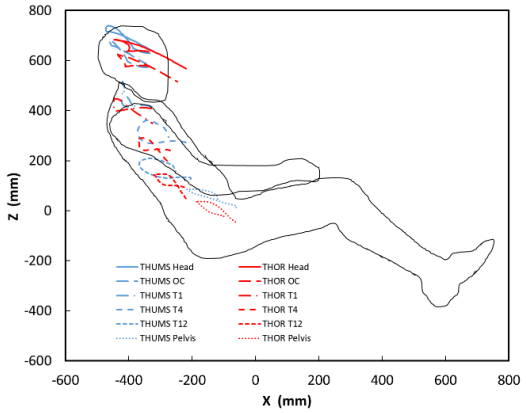

Figure 7. Trajectory comparison of THUMS and THOR-50M in 33° seatback angle, rearward facing

Head

The head acceleration for THUMS at 23° angle is much higher than any other cases in this study, shown in Figure 46 in Appendix II. To the author's knowledge, the biofidelity of both THOR-50M and the THUMS in rear impact was not evaluated in the past, there was not enough information to draw conclusion whether the high resultant head acceleration represents the production seat test data. However, attention should be paid to the head restraint system to address the potential head injury in high-speed rear impact conditions.

The rotations in y direction have similar magnitudes in loading stage and the THUMS rebound in y rotation was much higher, see Figure 48 in Appendix II. For the head rotation in z direction, the THUMS has much higher magnitude than the THOR-50M, see Figure 49. THOR-50M neck torsion response is much more stiffer than a human in the first 45° rotation from neutral forward position, where the human neck experiences a very low resistance in such a range [8][9].

Thoracic Displacement – Upper Left and Upper Right

It was noticed that the thorax displacement in x-direction at the upper left IR-TRACC attachment location is near 40 mm in the rear impact test condition, shown in Figure 50. It reached the peak earlier in THOR-50M than in THUMS, shown in Figure 50. The ribs of THUMS moved upward relative to the spine with a much higher magnitude, while THOR-50M moved downward with a very low magnitude, see Figure 52.

The displacements at upper right IR-TRACC location were similar to these at the upper left IR-TRACC location, see Figure 53 and Figure 55 in Appendix II.

Thorax Displacement – Lower Left and Lower Right

The x displacement at lower left IR-TRACC location was much higher in THOR than in THUMS for 43 degree seatback angle, see Figure 56 in Appendix II, while reversed in z displacement, see Figure 58. The higher the seatback angle is, the higher the thorax displacement. This was most likely due to the interaction with shoulder belt in the upward motion. The occupant torso would be more upright with a higher seatback angle. The displacement in THUMS was very sensitive to the seatback angle change while THOR-50M was much less sensitive.

The displacement at the lower right IR-TRACC was similar to the lower left IR-TRACC except for the y displacement. The y displacement indicated the THOR-50M and THUMS moved opposite directions, see Figure 57 and Figure 60 in Appendix II.

Abdomen Displacement

The abdomen x displacement is comparable between the two models in magnitude, see Figure 62 for the left and Figure 65 for the right side respectively. The THOR-50M stayed plateaued after it reached its maximum while the THUMS recovered back. In y and z directions, the THUMS had much higher displacement magnitudes, moving rightward in y direction and downward in z direction, see Figure 63 and Figure 64 for the left side and Figure 66 and Figure 67 for the right side respectively. It was observed that in the y direction, the displacement moved left (negative), opposite to the THOR-50M motion, see Figure 63 for the left side and Figure 66 for the right side in Appendix II.

Lower Thoracic Spine (Lumbar)

The lower thoracic spine x and z forces were higher, but y force was lower in THOR-50M, shown in Figure 68 through Figure 70 in Appendix II. The lower thoracic spine x force was not very sensitive to the seatback angle change except for THOR-50M with 43° seatback angle, shown in Figure 68. The moment measurement in THUMS were very low, especially in x and y directions, see Figure 71 and Figure 72.

CONCLUSIONS

FE models of the THOR-50M and midsize human male (THUMS) were used to study the occupant impact responses with different seatback angles in both forward and rearward facing configuration. The seating postures were based on a previous volunteer study. A US NCAP pulse with a 56 km/hour delta-V was used for the analysis.

In forward facing condition, the THUMS excursions in head, spine and pelvis were greater than THOR-50M. Head accelerations were comparable between the two models. The head rotation in x and z were higher in THUMS model. For the upper thoracic displacement at IR-TRACC attachment point, the displacements in x direction were similar between the two models. Higher displacements in y and z directions were observed for THUMS model. For the lower thoracic displacement at IR-TRACC locations, THOR-50M measurements were very low and the THUMS had positive x displacement, indicating the expansion instead of compression. This was caused by the organ movement when the chest was compressed. For the abdomen response, the magnitude of the displacement between the two models were comparable. The THOR-50M displacement stayed plateaued after reaching its maximum while THUMS recovered. For the pelvis, the acceleration had similar pattern and the THUMS output showed high oscillation magnitude. THUMS tended to submarine more than THOR-50M. The THOR-50M only submarined in the 43° seatback angle, evidenced by one or a combination of the animation, low ASIS load cell output (lap belt and ASIS engagement), low shoulder belt force and low seat pan force.

In rear facing, torso of the two models were restrained by the seatback and the excursions were relatively low. The head kinematics was strongly influenced by the interaction with the head restraint. The THUMS model had higher head acceleration and rotations. The upper thoracic resultant displacement was approximately 40 mm, which could be indicative of injury risk. THUMS upper thorax had high z displacement with a range 30-48 mm approximately. The lower thoracic displacement for THUMS was sensitive to the seatback angle change, and reached as high as 68 mm with 43° seatback angle. THOR-50M lower thoracic displacement was not sensitive to the seatback angle change. The abdomen displacement was similar in magnitude between the two FE models. The lumbar forces and moments for THOR-50M were much higher than THUMS, especially at 43° seatback angle.

LIMITATIONS

Neither FE model has been validated in reclined seating configurations. Consequently, the results in this study cannot be used to compare the biofidelity of the THUMS and THOR-50M. In addition, the Humanetics THOR-50M model was developed to fully represent the Humanetics THOR-50M ATD responses; no effort was made to improve its biofidelity beyond matching the physical dummy responses.

REFERENCES

[1] Lindman, M., Isaksson-Hellman, I., Strandroth, J., 2017. Basic numbers needed to understand the traffic safety effect of automated cars, IRCOBI Conference 2017, Antwerp, Belgium.

[2] Kitagawa, Y., Hayashi, S., Yamada, K., Gotoh, M., 2017. Occupant kinematics in simulated autonomous driving vehicle collisions: influence of seating positon, direction and angle, Stapp Car Crash Journal, Vol. 61 (November 2017), pp. 101-155.

[3] Reichert, R., Mohan, P., Marzougui, D., Kan, C. et al., "Validation of a Toyota Camry Finite Element Model for Multiple Impact Configurations," SAE Technical Paper 2016-01-1534, 2016, https://doi.org/10.4271/2016-01-1534.

[4] Kitagawa, Y., Yamada, K., Motojima, H., Yasuki, T., 2015. Consideration on Gender Difference of Whiplash Associated Disorder in Low Speed Rear Impact, Proceedings of IRCOBI Conference, pp. 233-245, Lyon, France.

[5] Kitagawa, Y., Yasuki, T., 2013. Correlation among Seatbelt Load, Chest Deflection, Rib Fracture and Internal Organ Strain in Frontal Collisions with Human Body Finite Element Models. Proceedings of IRCOBI Conference, pp. 282-316, Gothenburg, Sweden.

[6] Reed, M.P. and Ebert, S.M. 2018. “Effect of Recline on Passenger Posture and Belt Fit”. University of Michigan Transport Research Institute, Final Report UMTRI-2018-2, September 2018.

[7] Robins, D.H., 1983. Anthropometric specifications for mid-sized male dummy, vol. 2. UMTRI-83-53-2.

[8] Myers B.S., McElhaney J.H., Doherty B.J.m Paver J.G., Nightingale R.W., Ladd T.P. and Gray L., 1989. Responses of the human cervical spine to torsion, Proceedings of the 27th Stapp Car Crash Conference, November 1989.

[9] Kang, Y-S., Stammen, J., Moorhouse, K., Bolte, J., Head and neck responses of post mortem subjects in frontal, oblique, side and twist scenarios. 2018 International Research Council on the Biomechanics of Injury (IRCOBI) Conference Proceedings, 12 – 14 September 2018 – Athens, Greece.

APPENDIX I Forward Facing Data Plots

Head Acceleration and Rotation

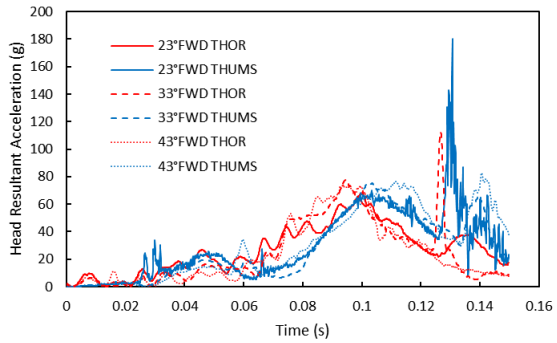

Figure 9. Head resultant accelerations

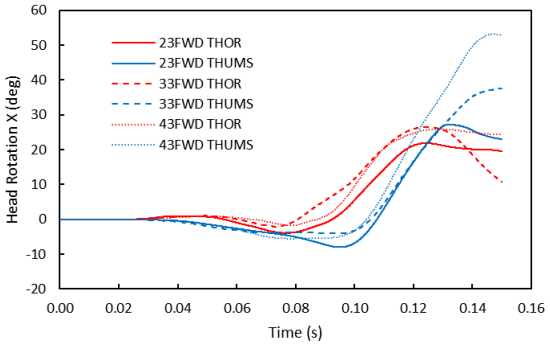

Figure 10. Head rotation x (integrated from angular velocity)

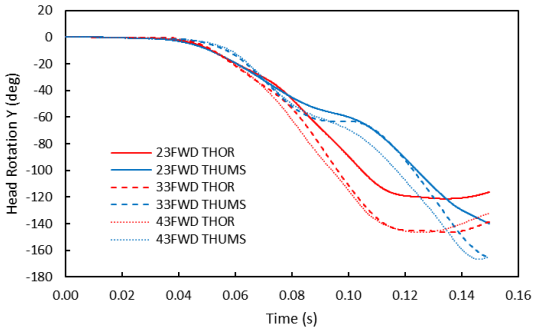

Figure 11. Head rotation y (integrated from angular velocity)

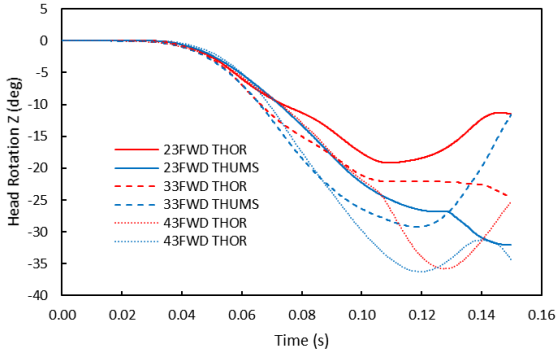

Figure 12. Head rotation z (integrated from angular velocity)

Thorax Displacement – Upper Left and Right

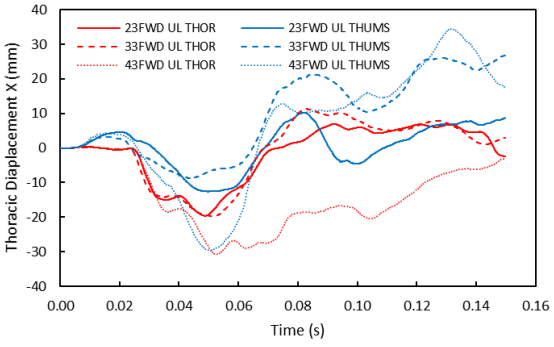

Figure 13. Thorax displacement x at upper left IR-TRACC front attachment point

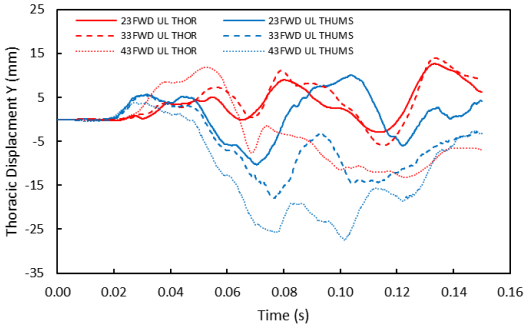

Figure 14. Thorax displacement y at upper left IR-TRACC front attachment point

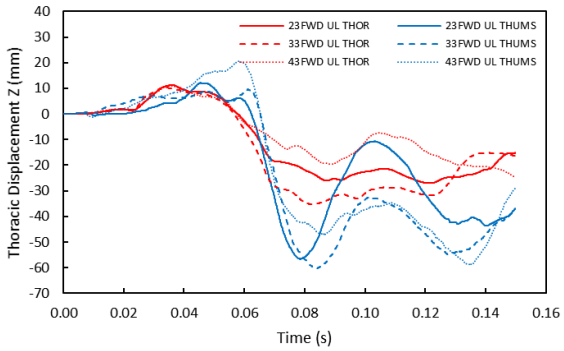

Figure 15 Thorax displacement z at upper left IR-TRACC front attachment point

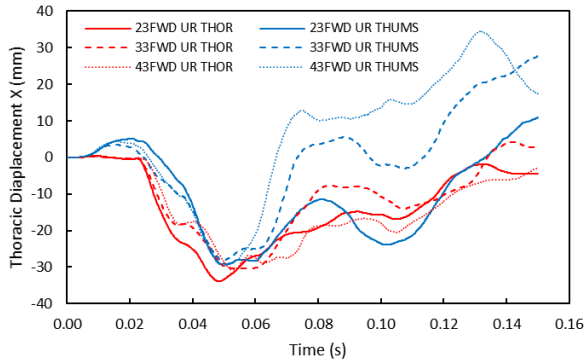

Figure 16. Displacement x at the upper right IR-TRACC front attachment point

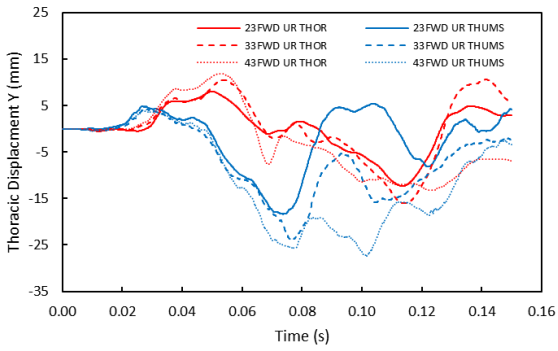

Figure 17. Displacement y at the upper right IR-TRACC front attachment point

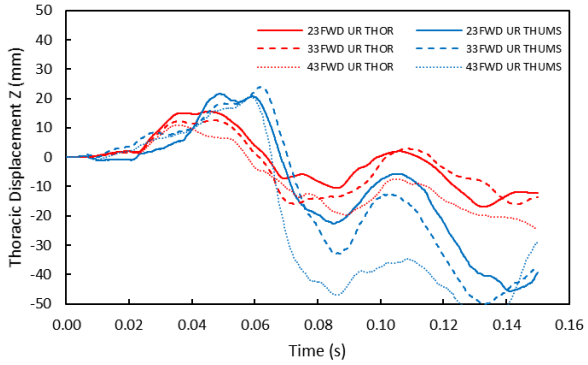

Figure 18. Displacement z at the upper right IR-TRACC front attachment point

Thorax Displacement – Lower Left and Right

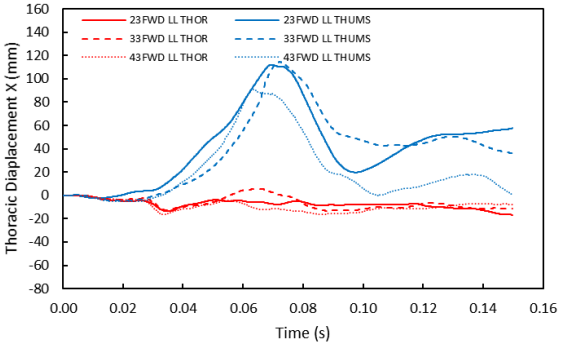

Figure 19. Displacement x at the lower left IR-TRACC front attachment point

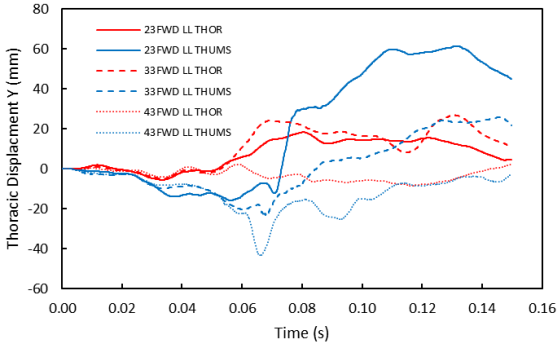

Figure 20. Displacement y at the lower left IR-TRACC front attachment point

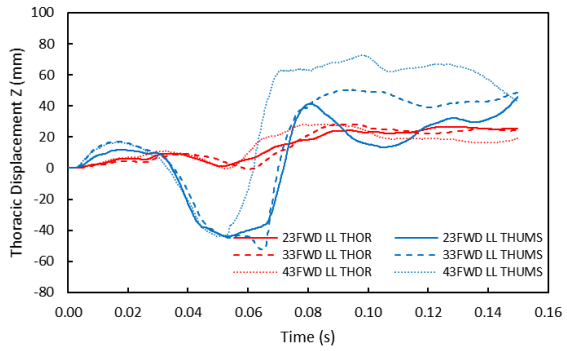

Figure 21. Displacement z at the lower left IR-TRACC front attachment point

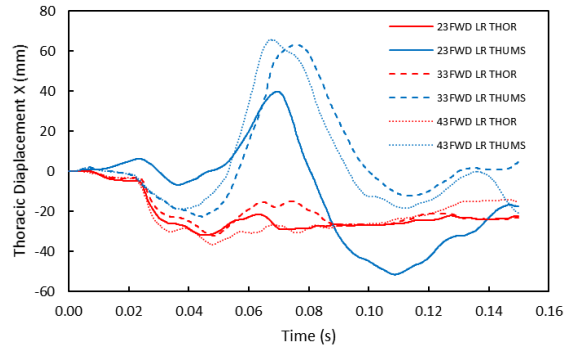

Figure 22. Displacement x at lower right IR-TRACC front attachment point

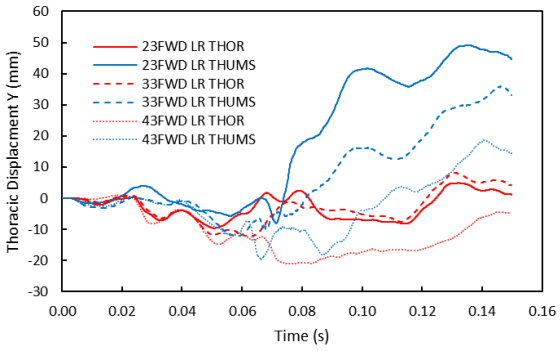

Figure 23. Displacement y at lower right IR-TRACC front attachment point

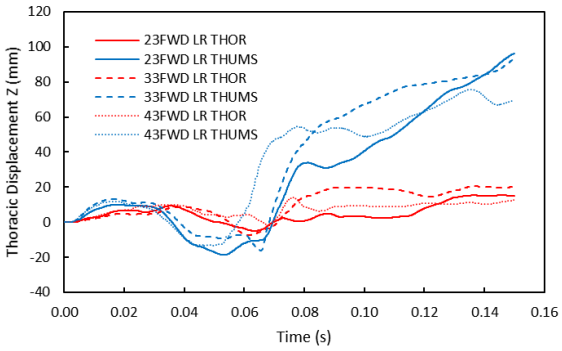

Figure 24. Displacement z at lower right IR-TRACC front attachment point

Abdomen Displacement – Left and Right

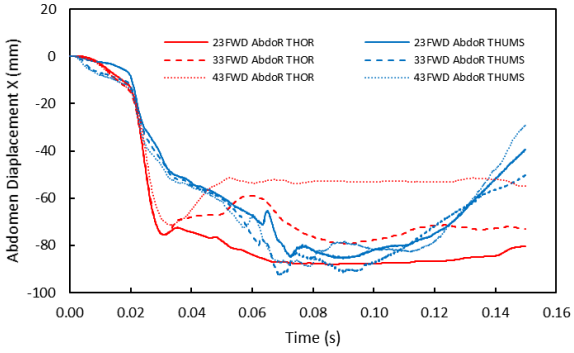

Figure 25. Displacement x at abdomen left IR-TRACC front attachment point

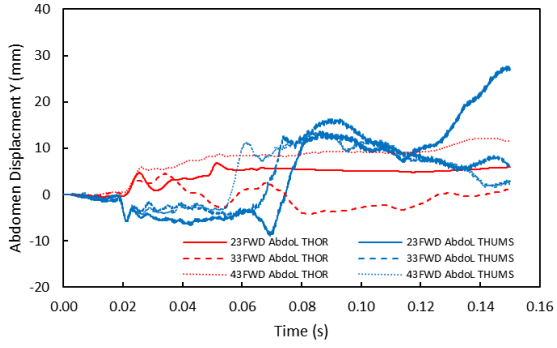

Figure 26. Displacement y at abdomen left IR-TRACC front attachment point

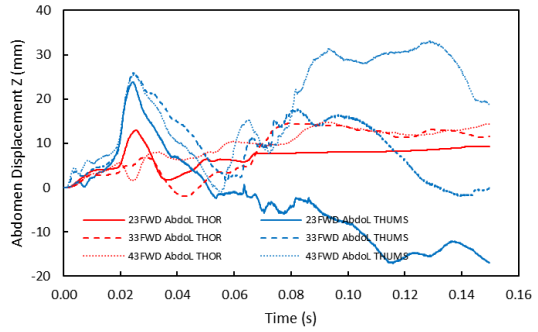

Figure 27 Displacement z at abdomen left IR-TRACC front attachment point

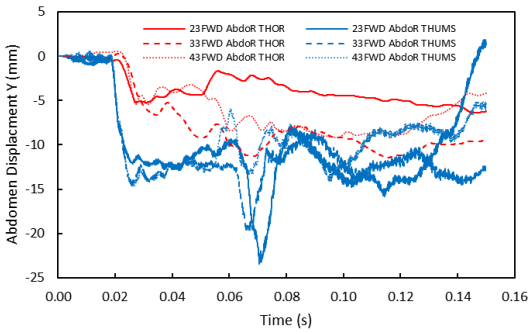

Figure 29 Displacement y at the right abdomen IR-TRACC attachment point

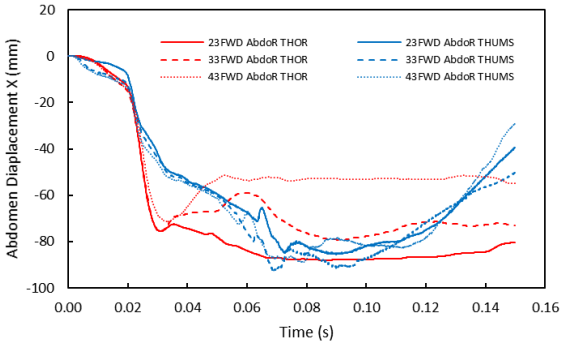

Figure 28. Displacement x at the right abdomen IR-TRACC attachment point

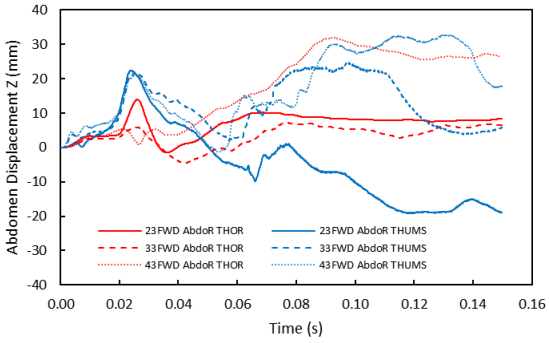

Figure 30. Displacement z at the right abdomen IR-TRACC attachment point

Pelvis

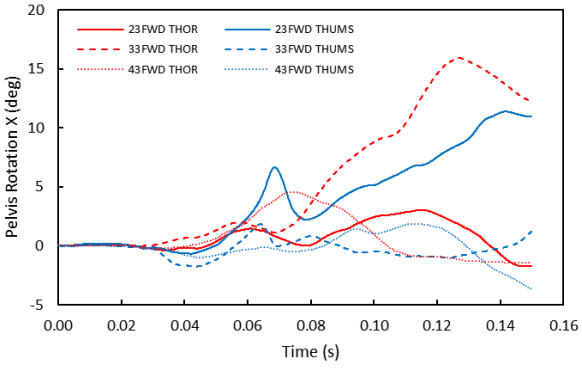

Figure 31. Pelvis bone rotation in x direction (integrated from angular rate)

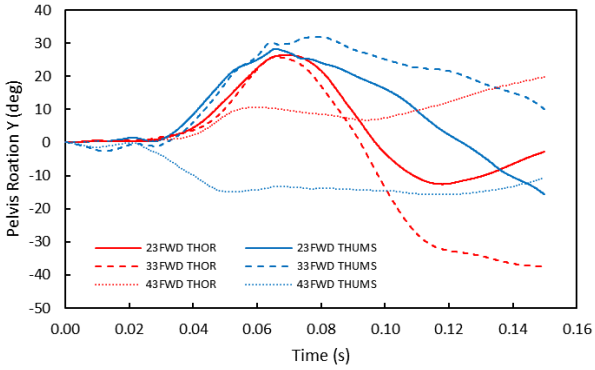

Figure 32. Pelvis rotation in y direction (integrated from angular rate)

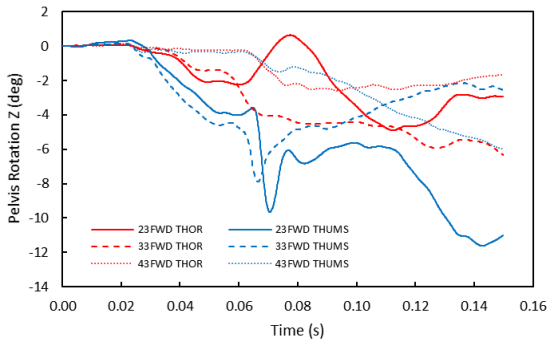

Figure 33. Pelvis rotation in z direction (integrated from angular rate)

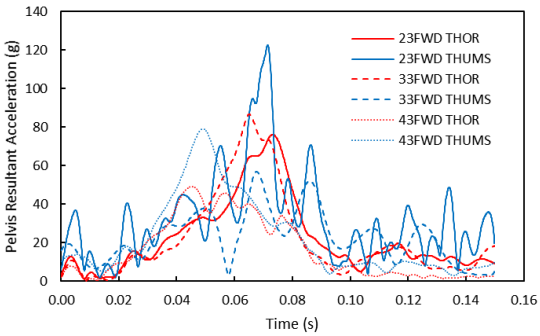

Figure 34. Pelvis resultant acceleration

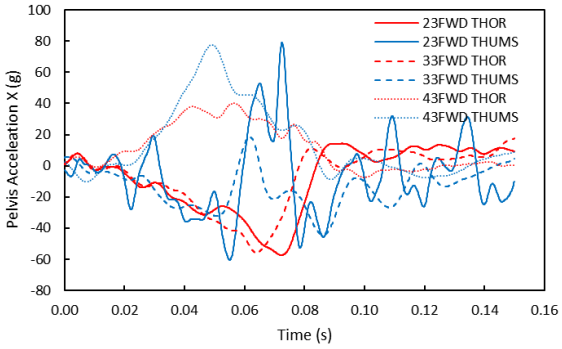

Figure 35. Pelvis acceleration in x direction

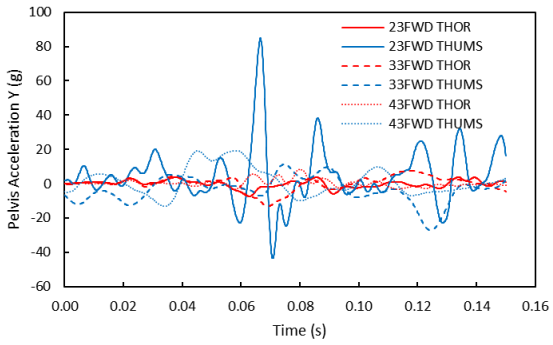

Figure 36. Pelvis acceleration in y direction

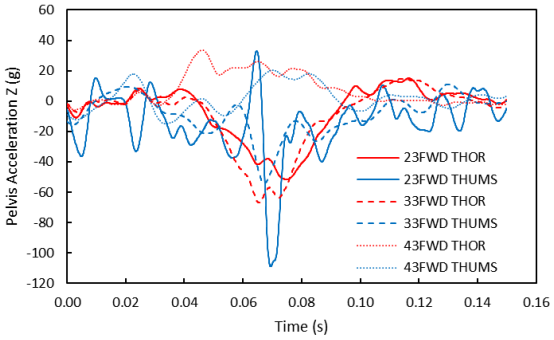

Figure 37. Pelvis acceleration in z direction

ASIS

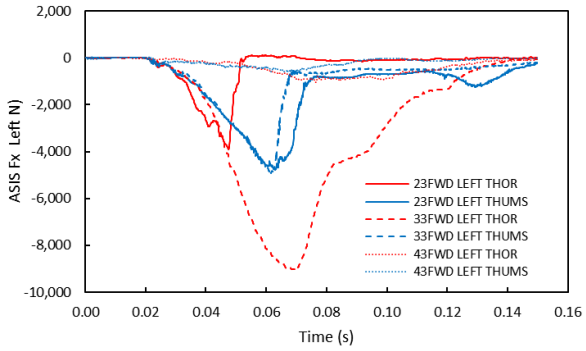

Figure 38. Force in x direction for the left A.S.I.S.

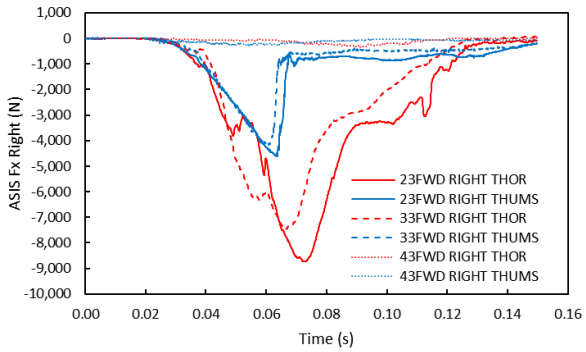

Figure 39. Force in x direction for the right A.S.I.S.

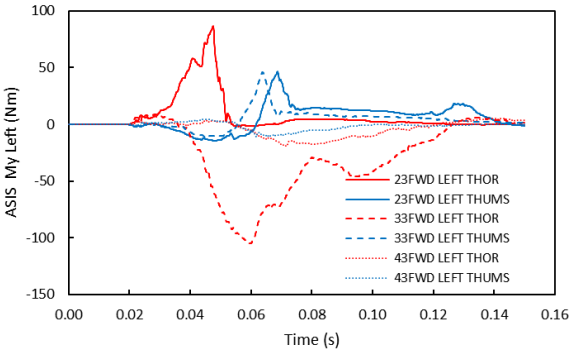

Figure 40. Moment in y direction for the left A.S.I.S

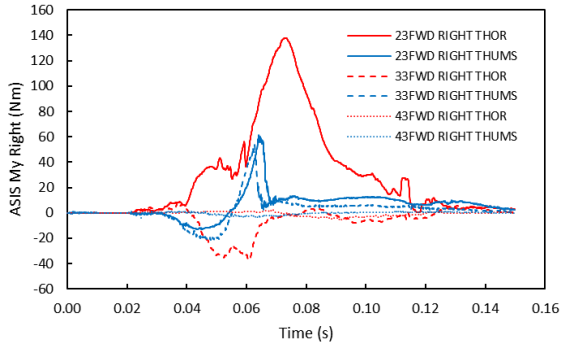

Figure 41. Moment in y direction for the right A.S.I.S.

Seat Belt

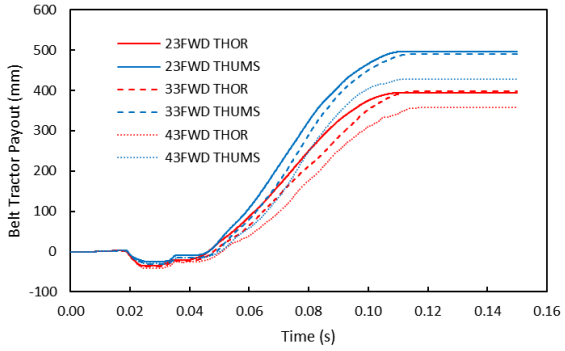

Figure 42. Shoulder belt tractor payout

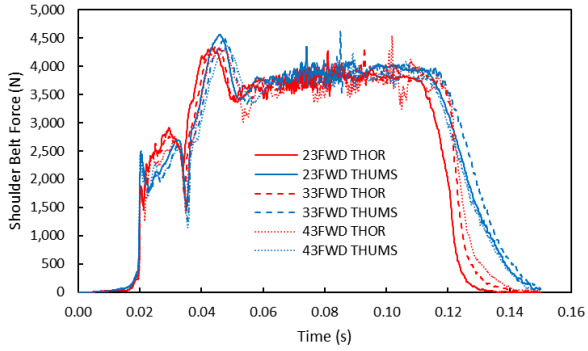

Figure 43. Shoulder belt force

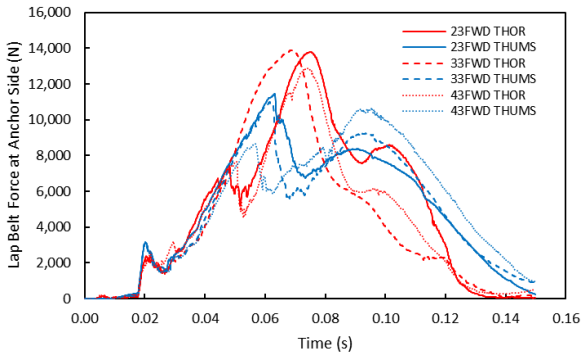

Figure 44. Lap belt force at anchor side

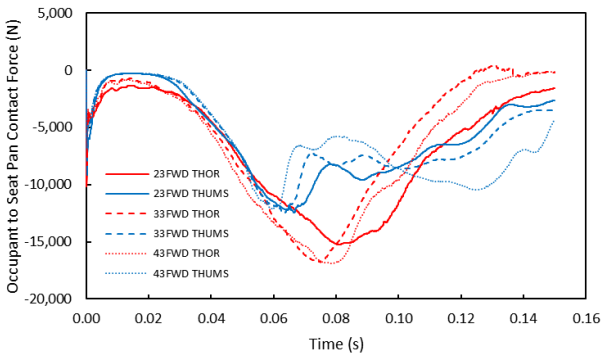

Figure 45. Occupant seat pan contact force

APPENDIX II Rear Facing Additional Plots

Head

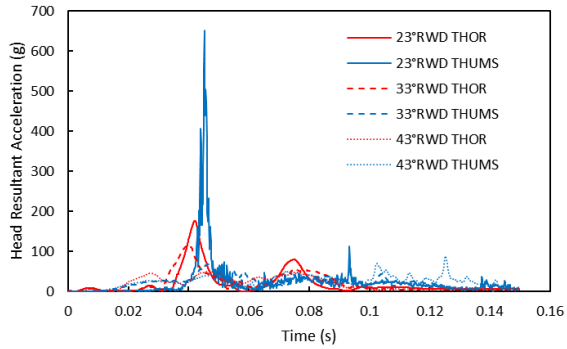

Figure 46. Head resultant acceleration

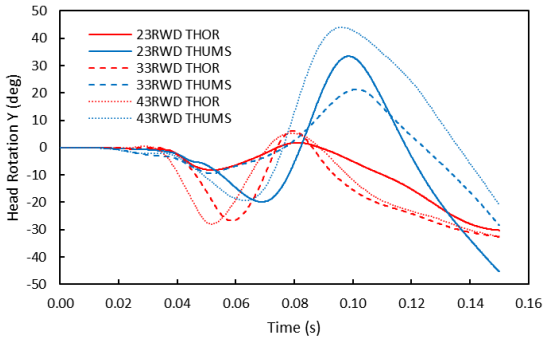

Figure 48. Head rotation y (integrated from angular rate)

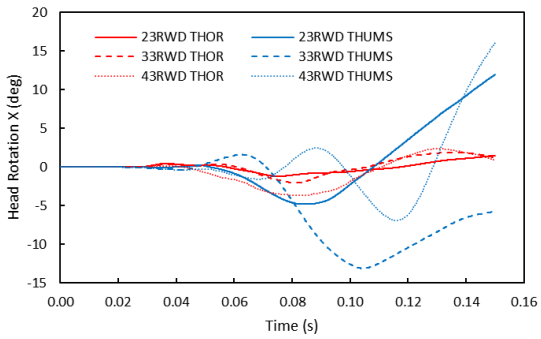

Figure 47. Head rotation x (integrated from angular rate)

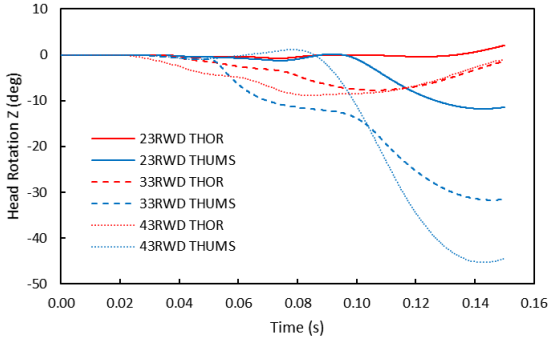

Figure 49. Head rotation z (integrated from angular rate)

Thorax Displacement – Upper Left and Right

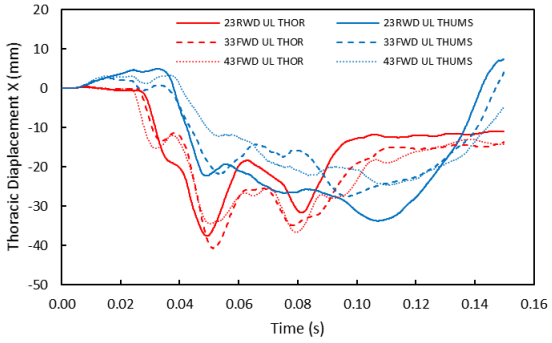

Figure 50. Displacement x at upper left IR-TRACC front attachment location

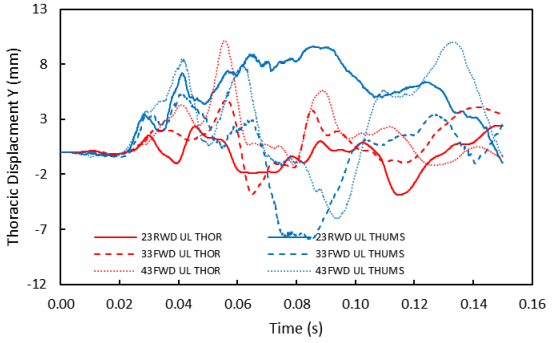

Figure 51. Displacement y at the upper left IR-TRACC front attachment location

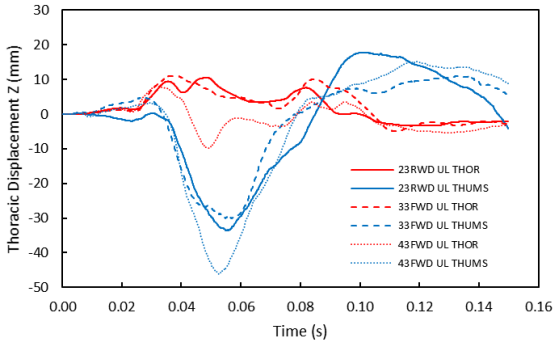

Figure 52. Displacement z at upper left IR-TRACC front attachment location

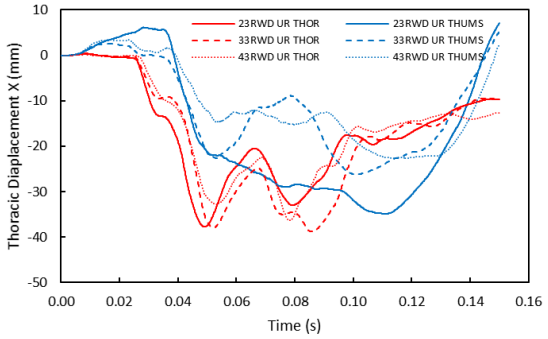

Figure 53. Displacement x at upper right IR-TRACC location

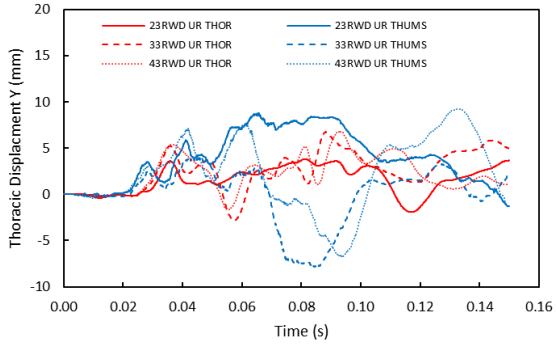

Figure 54. Displacement y at the upper right IR-TRACC location

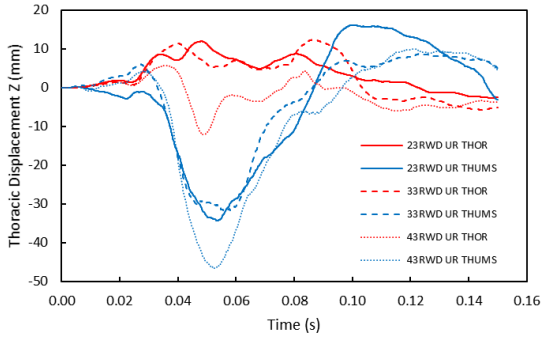

Figure 55. Displacement z at the upper right IR-TRACC location

Thorax Displacement – Lower Left and Right

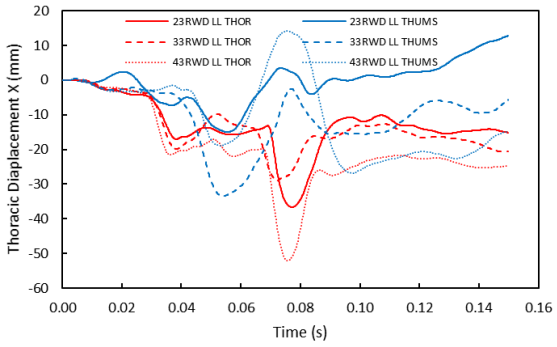

Figure 56. Displacement x at lower left IR-TRACC front attachment location

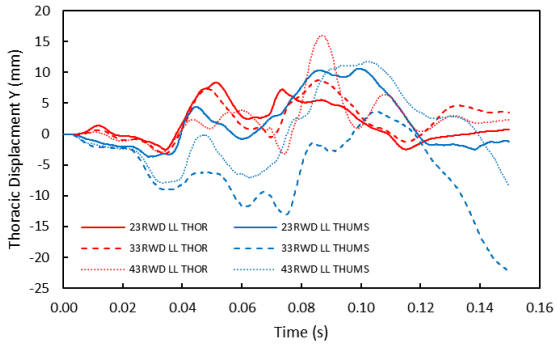

Figure 57. Displacement y at lower left IR-TRACC front attachment location

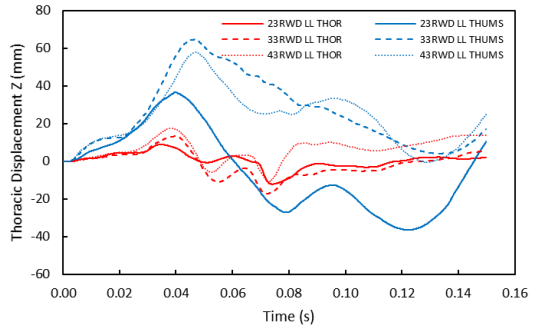

Figure 58. Displacement z at the lower left IR-TRACC attachment location

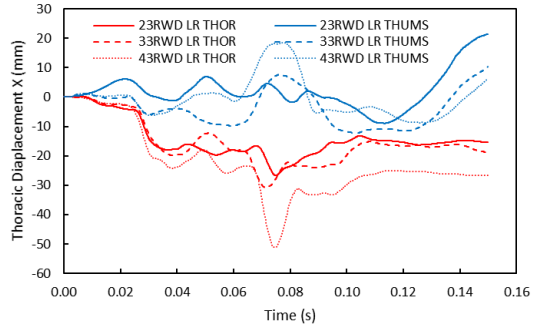

Figure 59. Displacement x at lower right IR-TRACC front attachment location

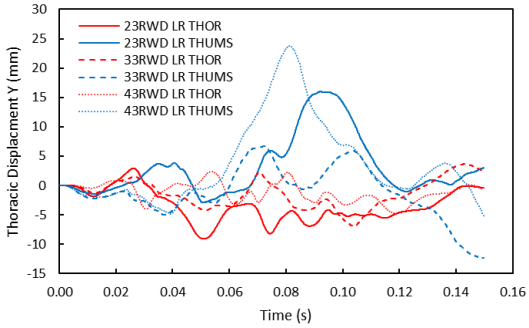

Figure 60. Displacement y at the lower right IR-TRACC front attachment location

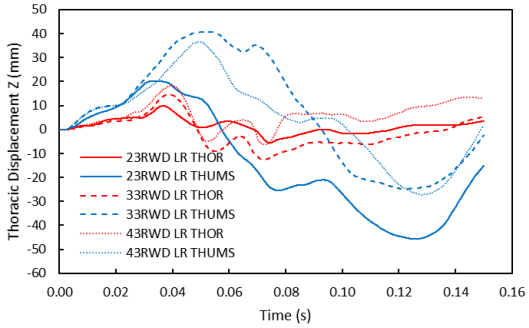

Figure 61. Displacement z at the lower right IR-TRACC front attachment location

Abdomen Displacement – Left and Right

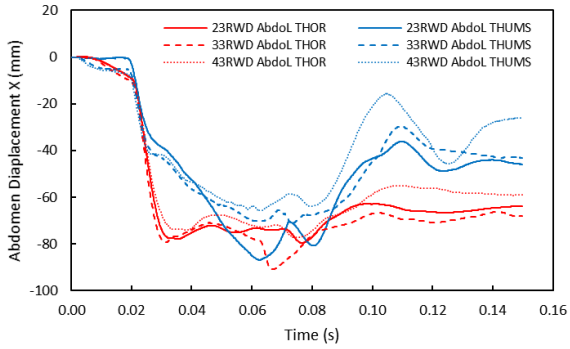

Figure 62. Displacement x at abdomen left IR-TRACC front attachment position

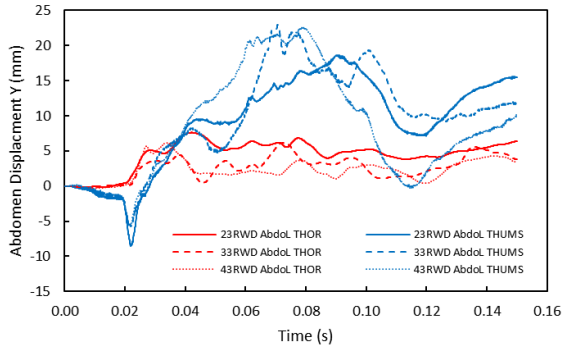

Figure 63. Displacement y at abdomen right IR-TRACC front attachment position

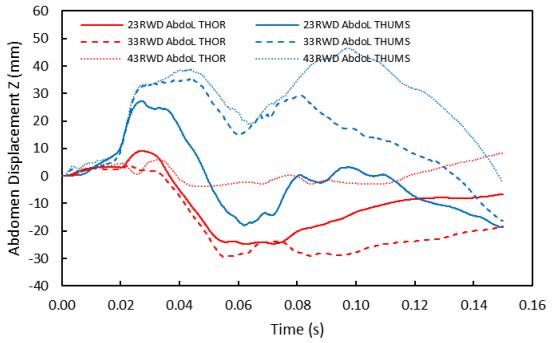

Figure 64. Displacement z at abdomen right IR-TRACC front attachment position

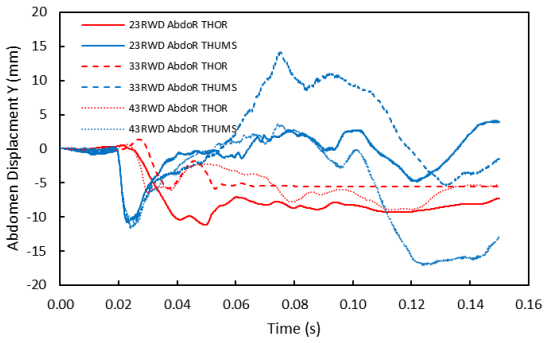

Figure 66. Displacement y at abdomen right IR-TRACC front attachment location

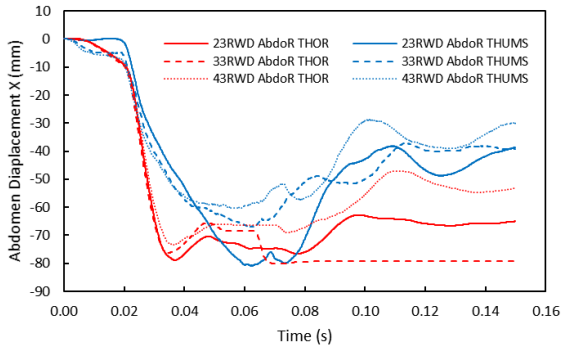

Figure 65. Displacement x at the abdomen right IR-TRACC front attachment location

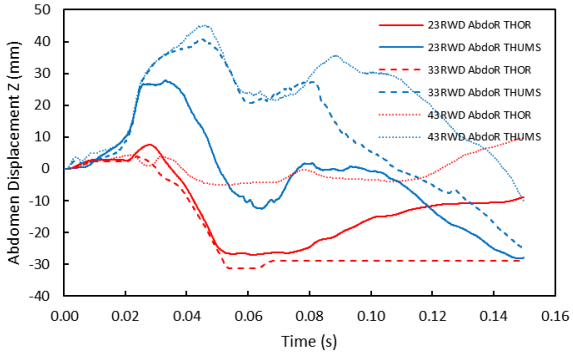

Figure 67. Displacement z at the abdomen right IR-TRACC front attachment location

Lumbar Spine

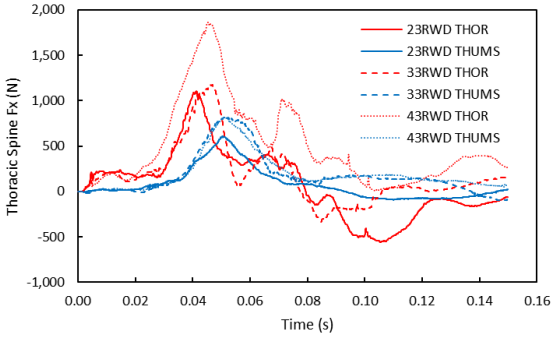

Figure 68. Lower thoracic spine force in x direction

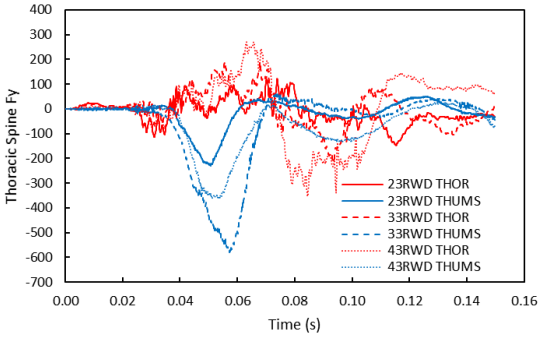

Figure 69. Lower thoracic spine force in y direction

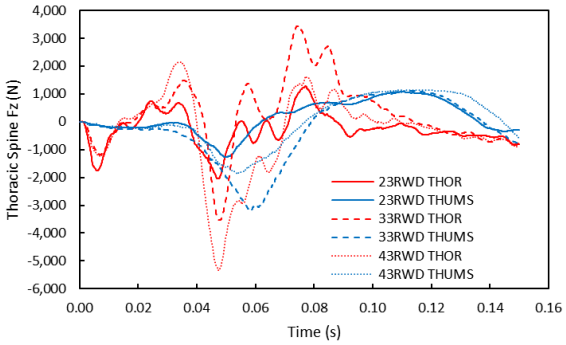

Figure 70. Lower thoracic spine force in z direction

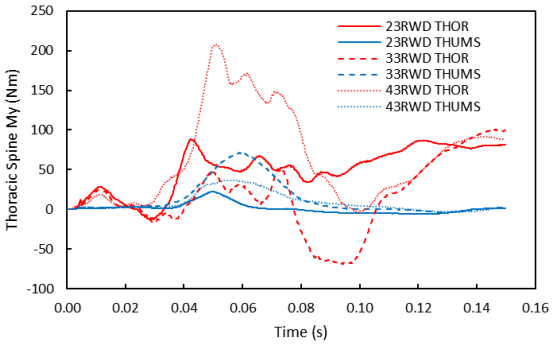

Figure 72. Lower thoracic spine moment in y direction

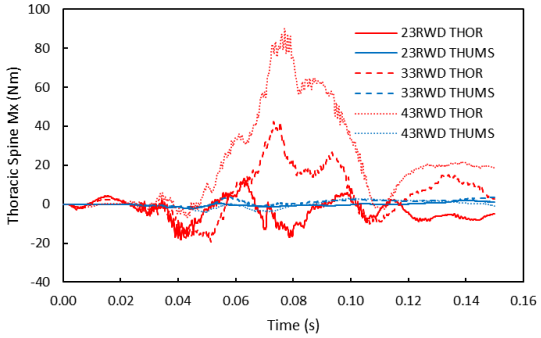

Figure 71. Lower thoracic spine moment in x direction

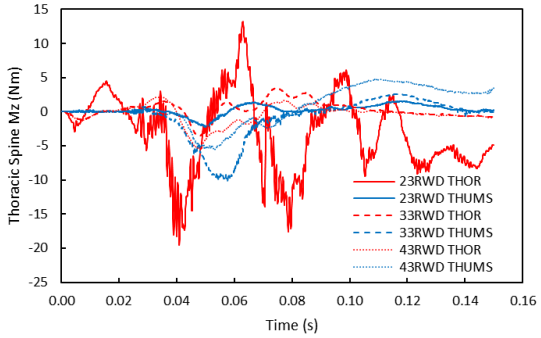

Figure 73. Lower thoracic spine moment in z direction